

FINITE ELEMENT MODELLING OF RECTANGULAR CONCRETE-FILLED STEEL TUBE STUB COLUMNS INCORPORATING HIGH STRENGTH AND ULTRA-HIGH STRENGTH MATERIALS UNDER CONCENTRIC AXIAL COMPRESSION

Son Thai^{a,b,*}, Ngo Huu Cuong^{a,b}, Dinh Van Thuat^c

^a*Faculty of Civil Engineering, Ho Chi Minh City University of Technology (HCMUT),
268 Ly Thuong Kiet street, District 10, Ho Chi Minh city, Vietnam*

^b*Vietnam National University Ho Chi Minh City,
Linh Trung ward, Thu Duc district, Ho Chi Minh city, Vietnam*

^c*Faculty of Building and Industrial Construction, Hanoi University of Civil Engineering,
55 Giai Phong road, Hai Ba Trung district, Hanoi, Vietnam*

Article history:

Received 02/9/2021, Revised 04/10/2021, Accepted 06/10/2021

Abstract

This study presents a unified approach to simulate the behavior of rectangular concrete-filled steel stub columns incorporating high strength and ultra-high strength materials subjected to concentric axial compression. The finite element model is developed based on Abaqus software, which is capable of accounting for geometrical nonlinearity, material plasticity, and interaction between multi-physics. The proposed model incorporates the influences of residual stress for welded-box steel sections and initial imperfection. A novel stress-strain relation of confined concrete is proposed to account for the composite action, which might increase the strength and ductility of infilled concrete under multi-axial compressive conditions. Various verification examples are conducted with wide ranges of geometrical and material properties. The simulation results show that the proposed model can accurately predict the ultimate strength, load-deformation relations, and failure mode of the experimental specimens.

Keywords: concrete-filled steel tube columns; stub columns; axial compression; finite element analysis; high strength materials.

[https://doi.org/10.31814/stce.huce\(nuce\)021-15\(4\)-07](https://doi.org/10.31814/stce.huce(nuce)021-15(4)-07) © 2021 Hanoi University of Civil Engineering (HUCE)

1. Introduction

In recent decades, Concrete-Filled Steel Tube (CFST) columns have been increasingly used in various residential and infrastructural structures such as high-rise buildings, bridges, and other industrial structures. This is due to the excellent structural performance of those structural members, such as high strength, high ductility, and large energy absorption capability. In recent year, the use of high strength and ultra-high strength steel and concrete materials in CFST columns have attracted great

*Corresponding author. *E-mail address:* son.thai@hcmut.edu.vn (Thai, S.)

attention from various researchers and structural engineering in practical applications [1]. In comparison to normal strength CFST columns, high strength CFST columns are found to be more attractive owing to their economical and architectural advantages from reducing the sizes of members and consequently the amount of material used. However, a recent investigation pointed out that the portion of previous studies on high strength CFST columns is still limited [2]. In addition, the current design codes for composite structures [3–5] are only applicable for normal strength steel and concrete (the yield strength of steel and concrete is limited to 460 MPa and 60 MPa, respectively). This is because of the shortage of experimental data and adequate investigations.

Pioneering investigations on structural response and design of high strength CFST were conducted by Uy [6, 7]. The results in those studies indicated that the Eurocode 4 [5] approach overestimated the ultimate strength of cross-sections in cases high strength steels are used. Sakino et al. [8] conducted a comprehensive experimental study on composite columns with normal strength and high strength materials. They also proposed design formulas to estimate the ultimate strength of composite columns based on the obtained results. Other previous experimental research on high strength CFST are the studies of Liu and his colleagues [9, 10], Yu et al. [11]. In general, it was found out in those studies that the provisions in current design codes conservatively predict the ultimate strength of the specimens made from high strength steel. Recently, some experimental studies on CFST columns with ultra-high strength concrete and steel have been conducted. In the studies of professor Liew's group [12–14], CFST specimens with steel yield strength up to 700 MPa and concrete compressive strength up to 170 MPa were used. They also pointed out that EC4 provisions reasonably estimate the strength of CFST columns if the confinement effect was considered. Other noticeable experimental investigations on CFST with ultra-high strength steel and concrete have been conducted by Khan et al. [15, 16], Chen et al. [17], Huang et al. [18], Nguyen et al. [19], and Cai et al. [20].

Due to the insufficiency of experimental data on high-strength and ultra-high strength CFST columns [2], the numerical investigation could be considered as an alternative approach to study the structural performance and application of such structures [21–23]. Although experimental investigation yields reliable results on the behavior of structural members, the approach is highly expensive and time-consuming. With the development of computer science and computational engineering techniques, numerical modeling offers an effective way to investigate the behavior of CFST columns without any limitations on geometrical and material parameters. Amongst the numerical modeling approaches, the Finite Element Method (FEM) is considered the most efficient and versatile technique that is widely employed in the engineering community. For CFST columns, it is well known that the composite actions of concrete core and outer steel tube are extremely complicated due to the multi-axial stress state and interaction between two materials. FEM allows the composite action to be considered carefully and provides a rational and accurate concrete model to describe the behavior of concrete and steel in multi-axial stress state and interaction conditions. However, it is found that previous simulation models based on FEM [21, 22, 24] were developed for CFST columns made from normal strength materials and high strength materials only, while only a few specimens with ultra high-strength concrete were considered, e.g. there are only 15 specimens with ultra-high strength material ($f'_c > 120$ MPa, $f_y > 700$ MPa) reported in [22]. It is noted that these test data is attained from the study of Liew et al. [12], they were also considered in [21] and our study with two nominated results. Therefore, this study aims to develop an accurate simulation model based on FEM to predict the strength and structural behavior of rectangular CFST stub columns fabricated by high strength and ultra-high strength materials. The effects of initial local imperfections and residual stresses in weld-boxed sections are also taken into account. Material plasticity and geometrical nonlinearity are

considered by the available tools in Abaqus software. A new empirical equation used to describe the confinement effect of the concrete core is proposed. Verifications are also conducted to prove the accuracy of the proposed approach with the test data collected in the literature.

2. Modelling techniques

2.1. General descriptions

In this study, a FEM model is developed based on Abaqus software [24] to predict the response of rectangular CFST stub columns under axial compressive loads. In general, the columns are modeled with exact dimensions reported in experimental data. The steel tube and concrete core are modeled by using the S4R (four-node shell element with reduced integration) and C3D8R (8-node linear brick element with reduced integration and hourglass control). A mesh convergence study was conducted and the optimal mesh size that produces converged solutions with minimum computing time is $H/15$ for steel tube and $H/12$ for concrete core, respectively, where H is the height of columns' section as depicted in Fig. 1. For cold-formed and hot-rolled sections, a finer mesh is employed at the corner sections to ensure the round geometry.

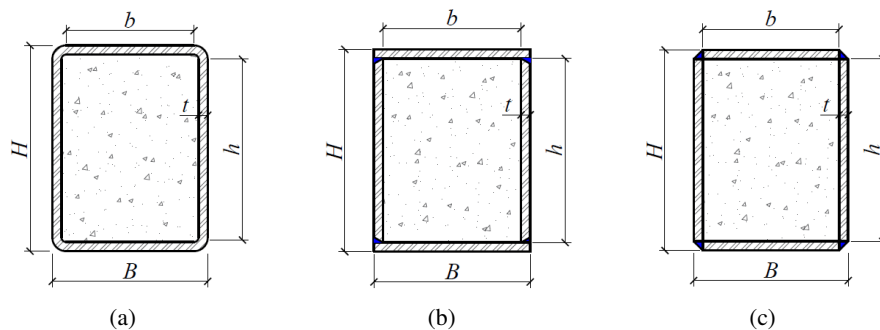


Figure 1. Typical cross-section of rectangular CFST columns
(a) cold-formed steel section, (b) and (c) welded-box steel sections

For the input data of steel and concrete, the engineering stress-strain curves are converted to true stress and logarithmic plastic strain by

$$\sigma_{true} = \sigma(1 + \varepsilon); \quad \varepsilon_{true}^{pl} = \ln(1 + \varepsilon) - \frac{\sigma_{true}}{E} \quad (1)$$

The interaction between steel stub and concrete core is simulated using the interaction algorithm in Abaqus, in which the small-sliding formulation is used and contact pair consists of the outer surface of concrete core and the inner surface of steel tube. In the interactive definition pop-up, the former is set mater surface and the latter is defined as slave surface. The interactive properties include normal and tangent behavior. The normal response is stimulated by the “hard” contact option to allow for the separation of two surfaces with no adhesive condition after contact and no penetration between two surfaces. A friction coefficient of 0.6 is employed to define the tangential behavior, which is based on the Coulomb friction model. It is noted that the value of the friction coefficient does not affect the situation results but influences the convergence problem [25].

The influence of initial imperfection is taken into account in the present study. This effect is considered by assign a local imperfection of $B/1000$ to the steel tube [21] by using the *Imperfection

keyword in Abaqus. The shape of the local imperfection is assumed to be the first buckling mode shape, which is obtained by conducting an eigenvalue buckling analysis. Illustrations for the initial imperfection of steel tubes are presented in Fig. 2.

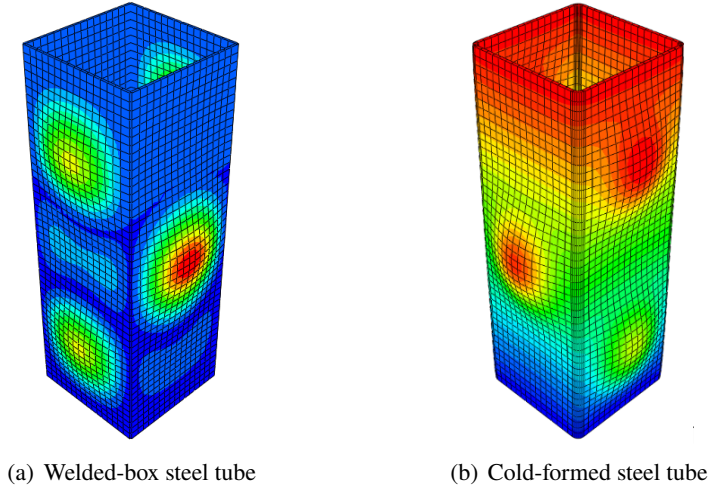


Figure 2. First-buckling mode shapes used as initial imperfection

Loading and boundary conditions in the simulation model are defined by using the rigid body constant technique provided in Abaqus. The top and bottom surfaces of the columns are tied to corresponding reference points at the center of each end. This assignment restrains the end section planar during the analysis as depicted in the test program for stub columns, therefore, the end-plates or stiffeners are not necessary to be included in the simulation model. Additionally, the boundary condition and loading condition are assigned to those reference points, where the cramped conditions are defined at the bottom and top reference points except axial displacement at the load end. The nonlinear solver based on the Newton-Raphson iterative technique with displacement-control method is utilized to trace the load-displacement response.

2.2. Material model of structural steel

For welded-box and hot-rolled steel jackets, the elastic-perfectly plastic model is employed to simulate the stress-strain relation of steel materials:

$$\sigma = \begin{cases} E_s \varepsilon & \text{for } \varepsilon \leq \varepsilon_y \\ f_y & \text{for } \varepsilon > \varepsilon_y \end{cases} \quad (2)$$

in which f_y is the yield strength and E_s is the elastic modulus of structural steel and can be taken as 200000 MPa in case no information is reported.

For the cold-formed steel, the stress-strain relations of flat and corner regions are taken separately due to the forming process. The elastic-perfectly plastic model is also employed and the model proposed by Gardner and Yun [26] for the rounded relations is adopted in this study as expressed in the following equations

$$\begin{aligned} \varepsilon &= \frac{\sigma}{E_s} + 0.002 \left(\frac{\sigma}{f_y} \right)^n & \text{for } f \leq f_y \\ \sigma &= f_y & \text{for } \varepsilon > \varepsilon_{0.2} \end{aligned} \quad (3)$$

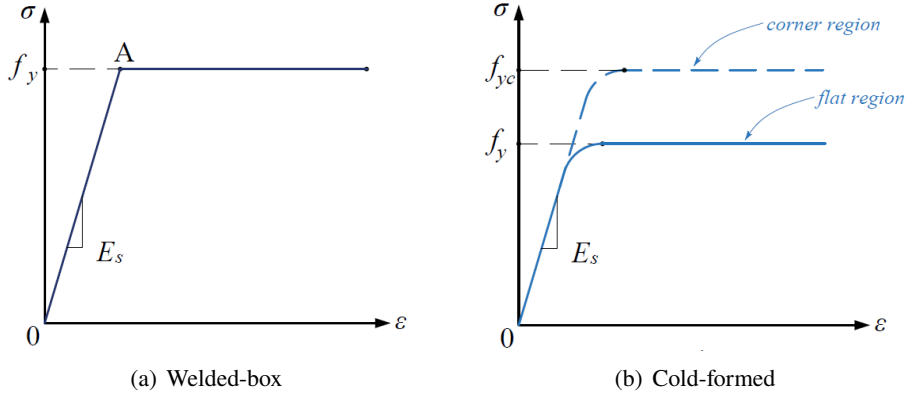


Figure 3. Stress-strain relations of steel

where f_y is replaced by f_{yc} for the corner regions to account for the strength enhancement due to forming procedure. The increment in yield strength is considered by using the model proposed by Rossi et al. [27] as follows

$$f_{yc} = p (\varepsilon_{c,av} + \varepsilon_{0.2})^q \leq f_u \quad (4)$$

where

$$\varepsilon_{f,av} = \left[\frac{t}{900} \right] + \left[\frac{\pi t}{2(B + H - 2t)} \right]; \quad \varepsilon_{c,av} = \frac{t}{2(2r_i + t)}; \quad p = \frac{f_y}{\varepsilon_{0.2}^q}; \quad q = \frac{\ln(f_y/f_u)}{\ln(\varepsilon_{0.2}/\varepsilon_u)} \quad (5)$$

in which r_i is the inner radius of corner regions and can be taken $r_i = t$ if $t \leq 6$ mm, $r_i = 1.5t$ if $6 \text{ mm} < t \leq 10$ mm, and $r_i = 2t$ if $t > 10$ mm. Other parameters in the model of Gardner and Yun [26] are given as follows: $n = 7.6$ for flat regions and $n = 7.0$ for corner regions, E_s can be taken as 203000 MPa when the elastic modulus of steel is not given, and

$$\varepsilon_{0.2} = 0.002 + \frac{f_y}{E_s} \quad (6)$$

In FE models, the corner regions are modeled with an extended distance of $2t$ as suggested by Yun and Gardner [28]. The steel with an enhanced yield strength (corner regions f_{yc}) and reported yield strength are assigned separately in the tubes' section as depicted in Fig. 4(b).

For the welded-box section, it is well-documented that the influence of membrane residual stresses along the welding lines induced by the welding process is essential and needed to be taken into account in simulation models. In this study, the residual stress in the welded-box section can be taken as follows based on Huang et al. [29] for high-strength and taken into consideration in Abaqus by using the keyword *INITIAL CONDITION. The distribution of membrane residual stress is illustrated in Fig. 4(a) and the magnitude of tensile (σ_{rt}) and compressive (σ_{rc}) stresses are calculated as follows

$$\sigma_{rt} = f_y (0.3 \ln(t) + 0.3) \leq f_y; \quad \sigma_{rc} = 2\sigma_{rt} \times \frac{b_t}{b_c} \quad (7)$$

$$b_t = 6.5 \ln(t) + 2; \quad b_c = b - 2b_t \quad (8)$$

For cold-formed steel tubes, various experimental studies have reported that both membrane and flexural residual stresses appear in the steel sections due to the manufacturing process. However,

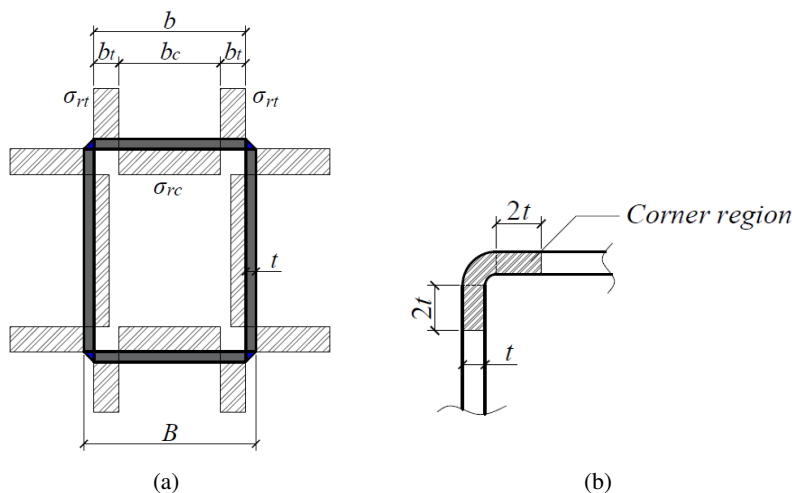


Figure 4. (a) Distributions of residual stress in welded-box sections, (b) Corner region in cold-formed sections

these residual stress are not explicitly considered in the FEM models for two reasons [28]: (1) the flexural residual stresses are inherently considered in the stress-strain curves obtained from tensile coupon tests to a large extent, and (2) the membrane residual stresses is relatively small and have an insignificant influence on the response of cold-formed steel.

It is worth noticing that the effects of residual stress and initial imperfection are minimized in CFST columns due to the appearance of infilled concrete. However, these effects might become significant when high strength steel and slender steel tubes are considered in the simulation models. The effects of these factors will be discussed later in the following section of this study.

2.3. Material model of confined concrete

To simulate the mechanical behavior of infilled concrete in CFST columns, the Concrete Damage Plasticity (CDP) model available in Abaqus is employed. The CDP was developed by Lee and Fenves [30] based on the initial study of Lubiner et al. [31] to capture the failure mechanics of concrete in compression and tension, which are associated with stiffness degradation and inelastic deformations. In general, the CDP model is considered as a continuum, plasticity-based, damage model and based on the theory of plastic flow. By adopting a combination of non-associated multi-hardening plasticity and scalar damaged elasticity, the model is capable of describing the damage in concrete, including two failure mechanisms: tensile cracking and compressive crushing. These failure modes are evaluated via the damage parameters, which and is characterized by the reduction of elastic stiffness and take the values ranging from 0 (no damage) and 1 (fully damage).

In this study, the CFST columns are subjected to monotonic axial compressive load only, therefore the damage parameters of concrete are not considered and only plasticity response is investigated. The damage parameters should indeed be considered to carefully investigate the response of CFST columns in the post-peak stage, however, the damage of concrete is not considered in this study due to the following reasons: (1) concrete core in CFST columns under uniformly monotonic compressive loads, the inclusion of damage parameters could not be used as the compressive stress dominates the behaviour of concrete core and the unloading response of concrete, which depends on the damage parameters, is not considered (2) the concrete in CFST columns is under a triaxial compressive stage

during loading, and the spalling of concrete is restricted, (3) the composite action in CFST columns could enhance the strength and ductility of concrete, and hence reduce the damage, (4) CDP model in Abaqus might be incapable of modeling the concrete in large multi-axial compressive stage, therefore the use of damage parameters, in this case, might not appropriate, 5) various studies on FEM of stub CFST columns under axial compression also ignored the damage on the concrete but yielded good solutions.

For CFST columns, it is well-known that the concrete core is restrained to expand laterally and is confined due to the outer steel jacket. This confinement phenomenon is passive in nature and could increase the strength and ductility of the infilled concrete. This is because the concrete core is in a triaxial stress state when the composite action between the steel tube and concrete core is activated. However, the default CDP in Abaqus fails to provide an accurate simulation of concrete subjected to different multiaxial loading scenarios if the confining pressure less than four or five times the ultimate compressive stress in uniaxial compression loading [24, 32]. To deal with this limitation, two types of techniques have been proposed in the literature: (1) developing a user-defined function in Abaqus to account for the influence of confining pressure on CDP parameters, and (2) modifying the stress-strain curve of unconfined concrete obtained to account for the effect of confining pressure. Amongst these two techniques, the latter has been widely used by different researchers thanks to its simplicity in implementation. In this study, a novel stress-strain relation of confined concrete in compression is also proposed.

In addition to the stress-strain curve of concrete on compression, other key parameters need defining in the CDP model are: the ratio of the second stress invariant on the tensile meridian to that on the compressive meridian (K_c), dilation angle (ψ), modulus of elasticity of concrete (E_c), Poisson's ratio (ν) flow potential eccentricity (e), the ratio of the compressive strength under biaxial loading to uniaxial compressive strength (f_{b0}/f'_c), viscosity parameter and tensile behavior of concrete. Discussions on the values of those parameters are given in the remaining parts of this subsection.

The empirical equation proposed by ACI 318-19 [33] is used to calculate the elastic modulus of concrete

$$E_c = 4700 \sqrt{f'_c} \tag{9}$$

where f'_c is the compressive strength of concrete determined from the standard test of 150x300mm cylinder specimens. The value of Poisson's ratio of concrete is taken as 0.2. The default values of flow potential eccentricity and viscous parameter are taken (0.1 and 0, respectively) as recommended by Tao *et al.* [21].

For the stress-strain relation of confined concrete, a two-stage model is proposed in this study to present the strain-hardening and softening rule of compressive concrete confined by the steel tube. In the hardening stage, the stress-strain model proposed by Hognestad [34] is employed

$$\sigma = f_{cc} \left[2 \frac{\varepsilon}{\varepsilon_{cc}} - \left(\frac{\varepsilon}{\varepsilon_{cc}} \right)^2 \right] \quad \text{for } 0 \leq \varepsilon \leq \varepsilon_{cc} \tag{10}$$

where f_{cc} is the peak compressive strength of confined concrete as depicted in Fig. 5. These values are calculated by the following formulas, which

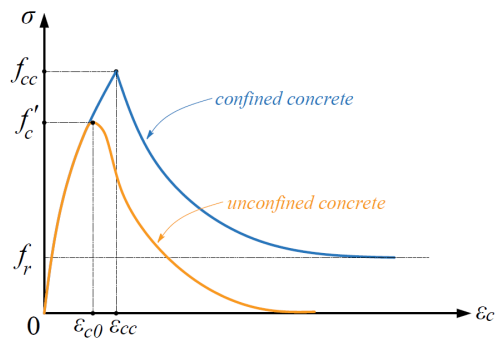


Figure 5. Stress-strain relation of confined concrete

are developed based on nonlinear regression analysis by considering the influences of section slenderness (B_{eq}/t), concrete strength f'_c and confinement factor ξ_c on confining pressures, which are obtained from trial simulations

$$\frac{f_{cc}}{f'_c} = \frac{5.1\xi_c^{0.71}}{(171.5 - f'_c)^{0.43}} \exp\left(-0.012\frac{B_{eq}}{t}\right) \geq 1 \quad (11)$$

and ε_{cc} is the corresponding strain, which is calculated by the proposed formula of Samani and Attard [35]

$$\frac{\varepsilon_{cc}}{\varepsilon_{c0}} = e^k; \quad k = (2.9224 - 0.00367f'_c) \left(\frac{f_l}{f'_c}\right)^{(0.3214+0.002f'_c)} \quad (12)$$

in which ε_{c0} is the strain at peak stress of unconfined concrete f'_c , f_l is defined as follow

$$f_l = \frac{\xi_c^{-0.2}(-70000 + 250f_y)e^{-0.025\frac{B_{eq}}{t}}}{430000 + 45(f'_c)^{0.9}} \quad (13)$$

ε_{c0} is the strain at peak stress of unconfined concrete is obtained from Tasdemir et al. [36]

$$\varepsilon_{c0} = 0.00076 + \sqrt{(0.626f'_c - 4.33) \times 10^{-7}} \quad (14)$$

and

$$B_{eq} = \sqrt{\frac{(B^2 + H^2)}{2}}; \quad \xi_c = \frac{A_s f_y}{A_c f'_c} \quad (15)$$

The softening stage is described by using the exponential function proposed by Binichi [37] as

$$\sigma(\varepsilon) = f_r + (f'_c - f_r) \exp\left[-\left(\frac{\varepsilon - \varepsilon_{cc}}{\alpha}\right)^\beta\right] \quad \text{for } \varepsilon > \varepsilon_{cc} \quad (16)$$

where f_r is the residual stress, which is defined as

$$f_r = \left(0.1 + \frac{1}{(B_{eq} - 10)^{1.74}}\right) f'_c \quad (17)$$

The parameters α and β are taken as proposed by Tao et al. [25] as follows

$$\alpha = 0.005 + 0.0075\xi_c; \quad \beta = 0.92 \quad (18)$$

Other parameters for the CDP model can be taken based on Tao et al. [25] as follows

$$\psi = 40^\circ; \quad f_{b0}/f'_c = 1.5(f'_c)^{-0.075}; \quad K_c = \frac{5.5}{5 + 2(f'_c)^{0.075}} \quad (19)$$

The tensile strength of concrete can be calculated based on the compressive strength of unconfined concrete based on the suggestion of ACI 224.2 R92 [38] as

$$f_t = 0.12\sqrt{2400f'_c} \quad (20)$$

The concrete tension is assumed to behave linearly up until the tensile strength f_t , then the tensile softening response is characterized using fracture energy based on the stress-crack width and displacement model of Hillerborg et al. [39], which is reported to be capable of preventing mesh-sensitivity and enhance numerical convergence. The strain energy of concrete can be calculated as suggested by fib 2010 code [40] as follows

$$G_f = 0.03(f'_c/10)^{0.7} \text{ (N/m)} \quad (21)$$

3. Verification of finite element model

In this section, the results obtained from current developed FEM models are verified against experimental data of rectangular CFST stub columns under axial compression. Twenty-seven tests are collected from different experimental studies of CFST columns incorporating high strength and ultra-high strength materials. The tested specimens include welded-box, hot-rolled, and cold-formed steel jackets. As presented in Table 1, the selected specimens have the width ranging from 50.9 to 305 mm and the width-to-thickness ratio ranging from 12 to 50, the yield strength of steel tube ranges from 306.7 MPa to 1022 MPa, and the compressive strength of concrete varies from 54.5 MPa to 164.1 MPa. It is noted that all the compressive strength of concrete with different types of specimens should be converted into the compressive strength f'_c determined from 150×130 mm specimens. The conversion is based on the suggestion of Mansur and Islam [41] as follows

$$f'_c = 0.98f_{cyl100} - 3.49; \quad f'_c = \frac{f_{cube} - 9.94}{1.01}; \quad f'_c = \frac{f_{cube100} - 1.947}{1.031} \quad (22)$$

Table 1. Details of selected CFST stub specimens incorporating high strength and ultra-high strength materials

Reference	Specimen	B (mm)	H (mm)	t (mm)	L (mm)	f_y (MPa)	E_s (GPa)	f'_c (MPa)	f'_c type	Steel-section
Liew et al. [12]	SSH1-2	150	150	8	450	779	200	157.2	Cyl 100	Welded-box
Liew et al. [12]	SSH2-2	150	150	12	450	756	199	157.2	Cyl 100	Welded-box
Liu et al. [10]	C2-2	100.7	100.4	4.18	300	550	207	72.1	Cyl	Welded-box
Liu et al. [10]	C9-2	160.7	80.5	4.18	480	550	207	60.8	Cyl	Welded-box
Liu [9]	R7-1	106	106	4	320	495	206	89	Cyl	Welded-box
Liu [9]	R9-1	80	160	4	480	495	206	89	Cyl	Welded-box
Yu et al. [11]	S30-2	100	100	1.9	300	404	207	121.6	Cube	welded-box
Aslani et al. [42]	HSSC7	180	180	5	570	701	-	54.5	Cyl	Welded-box
Khan et al. [15]	CB20-SH(B)	109.06	109.06	4.93	360	762	-	100	Cyl	Welded-box
Xiong et al. [13]	S4	150	150	8	450	779	200	164.1	Cyl 100	Welded-box
Xiong et al. [13]	S9	150	150	12	450	756	200	164.1	Cyl 100	Welded-box
Yan et al. [43]	S8-7-120	100	100	6.8	300	599.5	-	124.8	Cube 100	welded-box
Yan et al. [43]	S9-7-140	100	100	6.8	300	599.5	-	141	Cube 100	welded-box
Nguyen et al. [19]	C35-150	111	111	3	333	723.7	194.9	150	Cyl	welded-box
Nguyen et al. [19]	C45-150	141	141	3	423	723.7	194.9	150	Cyl	Welded-box
Nguyen et al. [19]	C40-130	126	126	3	378	723.7	194.9	130.1	Cyl	Welded-box
Varma [44]	SC-32-80	305	305	8.9	1200	560	197	110	Cyl	Cold-formed
Varma [44]	SC-48-80	305	305	6.1	1200	660	194	110	Cyl	Cold-formed
Xiong et al. [13]	S12	150	150	12.5	450	446	201	157.2	Cyl 100	Hot rolled
Chen et al. [17]	SS2-3	100.4	100.4	3.79	300	306.7	-	130.8	Cyl	Cold-formed
Chen et al. [17]	SS3-3	100.7	100.7	7.63	300	371.6	-	130.8	Cyl	Cold-formed
Ibanez et al. [45]	S125×125×4_90	125	125	4	300	342.59	210	94.33	Cyl	Cold-formed
Cai et al. [20]	80×80×4-C120-B	80.3	80.4	3.98	240	1022	210	114.9	Cyl	Cold-formed
Cai et al. [20]	120×120×4-C80-B	121.8	121.8	3.91	359	991	206	85.7	Cyl	Cold-formed
Cai et al. [20]	100×50×4-C80-A	50.9	100.2	4	300	721	212	85.7	Cyl	Cold-formed
Cai et al. [20]	160×160×4-C120-A	161.2	162	4.04	480	629	215	114.9	Cyl	Cold-formed

As can be seen from Table 2 and Fig. 6, the predicted ultimate strength of CFST columns obtained from FEM agrees well with those reported in experimental programs with both normal strength and high-strength material. A mean value (μ) of 0.97 is obtained with a relatively small value of the coefficient of variation ($CoV = 0.05$). Additionally, the results in Table 2 show that the proposed model can accurately predict the strength of CFST columns for a wide range of confinement factor ξ_c and section slenderness ratio B_{eqt}/t . In addition, to validate the employment of the proposed model, the confining stress on the concrete core is also investigated. Herein, the maximum contact pressures (CPRSS variables) in the corner regions of the columns are reported to represent the confining pressure and these values are obtained when the column reaches its ultimate strength. This technique is employed

because the concrete core is passively confined by the steel jacket and the significant lateral deformation of the steel tubes are normally occurs in the post-peak stage. In general, it is seen in Table 2 that the ratio of contact pressure to the compressive strength of concrete (σ_{cont}/f'_c) is greater than 1/5 for all cases.

Table 2. Comparison between simulation and experimental results of ultimate strength

References	Specimen	B_{eq}/t	ξ_c	σ_{cont} (MPa)	σ_{cont}/f'_c	N_{exp} (kN)	N_{FEM} (kN)	N_{exp}/N_{FEM}
Liew et al. [12]	SSH1-2	18.75	1.31	50.85	0.32	6715	6631	1.01
Liew et al. [12]	SSH2-2	12.50	2.09	42.49	0.27	8452	8341.49	1.01
Liu et al. [10]	C2-2	24.06	1.45	39.13	0.54	1775	1774.72	1.00
Liu et al. [10]	C9-2	30.40	1.60	31.17	0.51	1820	1809.63	1.01
Liu [9]	R7-1	26.50	0.95	25.16	0.28	1749	1735.94	1.01
Liu [9]	R9-1	31.62	0.94	24.22	0.27	1878	1914.53	0.98
Yu et al. [11]	S30-2	52.63	0.29	29.19	0.24	1220	1297.35	0.94
Aslani et al. [42]	HSSC7	36.00	1.56	31.62	0.58	3882	3955.25	0.98
Khan et al. [15]	CB20-SH(B)	22.12	1.59	36.62	0.37	2632	2684.51	0.98
Xiong et al. [13]	S4	18.75	1.25	64.56	0.39	7276	7243.28	1.00
Xiong et al. [13]	S9	12.50	2.00	44.59	0.27	8730	8693.49	1.00
Yan et al. [43]	S8-7-120	14.71	1.76	57.22	0.46	2368.9	2482.66	0.95
Yan et al. [43]	S9-7-140	14.71	1.55	59.57	0.42	2492.1	2595.64	0.96
Nguyen et al. [19]	C35-150	37.00	0.57	87.36	0.58	2437	2465.57	0.99
Nguyen et al. [19]	C45-150	47.00	0.44	75.42	0.50	3131	3829.56	0.82
Nguyen et al. [19]	C40-130	42.00	0.57	82.16	0.63	2739	2885.93	0.95
Varma [44]	SC-32-80	34.27	0.65	96.85	0.88	14 116	15 318.6	0.92
Varma [44]	SC-48-80	50.00	0.51	88.27	0.80	12 307	14 076.4	0.87
Xiong et al. [13]	S12	12.00	1.30	73.08	0.46	5911	5819.85	1.02
Chen et al. [17]	SS2-3	26.49	0.40	91.90	0.70	1676	1681.41	1.00
Chen et al. [17]	SS3-3	13.20	1.11	87.37	0.67	2051	2056.53	1.00
Ibanez et al. [45]	S125×125×4_90	31.25	0.51	54.50	0.58	1882.5	1961.59	0.96
Cai et al. [20]	80×80×4-C120-B	20.19	2.06	64.51	0.56	1898	1853.81	1.02
Cai et al. [20]	120×120×4-C80-B	31.15	1.64	66.20	0.77	2853	2920.5	0.98
Cai et al. [20]	100×50×4-C80-A	19.87	2.43	70.14	0.82	1211	1183.1	1.02
Cai et al. [20]	160×160×4-C120-A	40.00	0.59	57.82	0.50	4062	4272.42	0.95
							$\mu =$	0.97
							$CoV =$	0.05

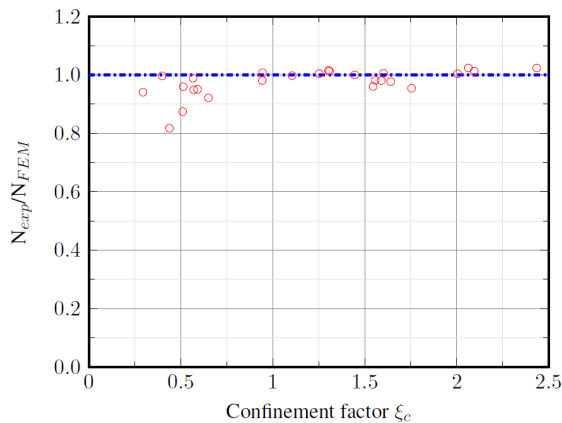


Figure 6. Comparison between predicted ultimate strength and experimental results

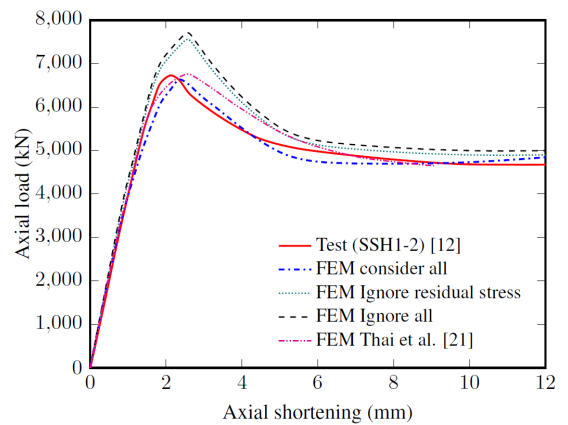


Figure 7. Influences of imperfection and residual stress on simulation results

To further verify the accuracy of the proposed simulation model, the load-shortening curves obtained from FEM and experimental results are compared in Figs. 7 and 8. In general, the predicted response obtained from FEM models is in reasonable agreement with experimental results, especially in terms of initial stiffness, ultimate strength, and the trend of softening branches. In Fig. 7, the influence of initial imperfection and residual stress on the simulation results are illustrated. It can be seen that the residual stress has a significant influence on the simulation results, while the inclusion of initial imperfection slightly affects the predicted ultimate strength. Therefore, the consideration of those effects is essential and should be accounted for in the simulation models to have a reasonable

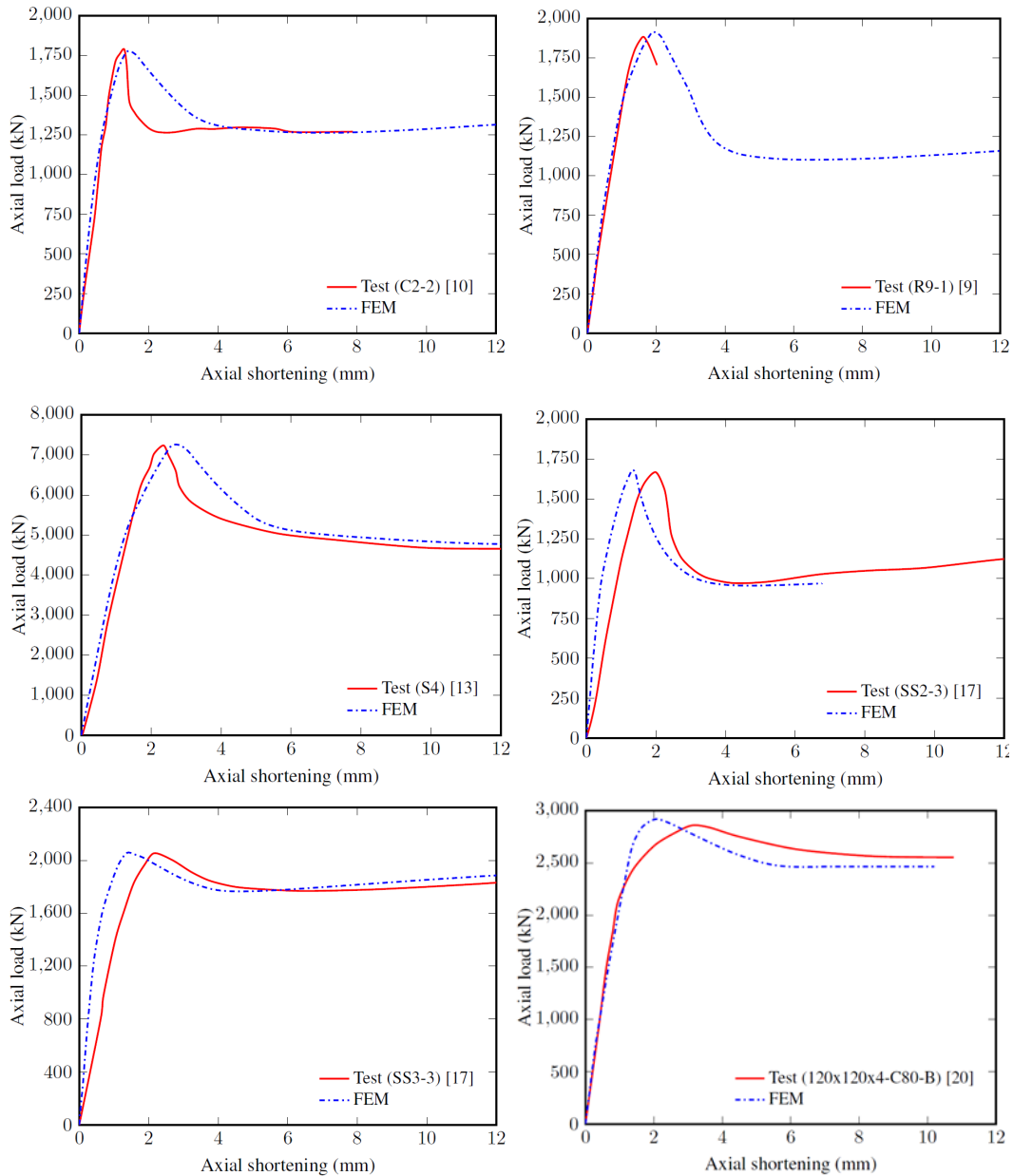


Figure 8. Comparison of the load-deformation curve

prediction. Additionally, it is seen that the simulation result obtained from the current model agrees well with one presented in Thai et al. [21], however, a better prediction for post-peak behavior is obtained with the proposed model in this study.

As illustrated in Fig. 8, the load-deformation curves of CFST columns can be divided into two stages. In the first stage, the compressive load is linearly proportional to the axial deformation up until the limit point, where the column reaches its ultimate strength. In the second stage, the strength of the columns drops with different trends depending on the confinement degree and slenderness ratio of the steel section. For specimens SS2-3 and SS3-3, the load-deflection curves in the elastic region obtained from FE simulations are slightly different from those presented by experimental programs. Various factors might be attributed to those differences, e.i. the errors during experimental programs when the axial deformation is measured, the unreliable value of elastic modulus obtained from the empirical equation proposed by ACI 318 for these cases. In general, the columns with a relatively large confinement factor ($\xi_c > 1.5$) and small slenderness ratio ($B_{eq}/t < 30$) have a flatter softening response as indicated in Table 2 and Fig. 8.

Finally, the failure mode shapes of columns obtained from simulations and experimental results are compared in Fig. 9. It is seen that the simulation results match well with the failure mode captured in the experimental programs. As expected, the failure mode of CFST stub columns under axial compression consists of a lateral expansion of columns' section and outer buckling of steel jackets in the mid-height of the specimens.

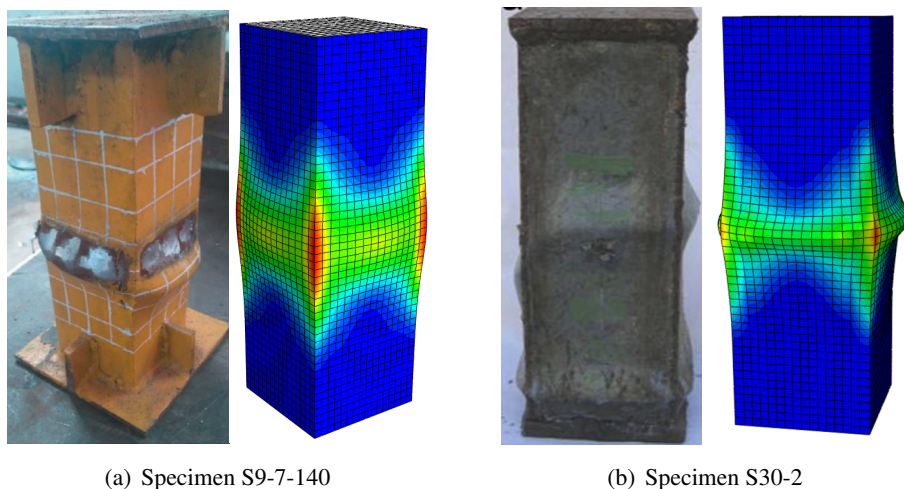


Figure 9. Comparison failure mode shapes

4. Conclusions

In this study, a Finite Element Model is developed based on Abaqus to analyze the behavior of rectangular CFST stub columns using high strength and ultra-high strength materials. A novel stress-strain relation confined concrete is proposed in this study to account for the composite effect, which might increase the strength and ductility of concrete. The present simulation model also considers the influences of residual stress for the welded-box section and initial imperfection. Verifications are conducted and the simulation results show that the proposed model can predict the ultimate strength, load-deformation relations, and failure modes of CFST columns for wide ranges of geometrical and material parameters.

Acknowledgments

This research is funded by Ho Chi Minh City University of Technology (HCMUT), VNU-HCM under grant number T-KTXD-2020-55. We acknowledge the support of time and facilities from Ho Chi Minh City University of Technology (HCMUT), VNU-HCM for this study.

References

- [1] Liew, J. Y. R., Xiong, M., Xiong, D. (2016). [Design of Concrete Filled Tubular Beam-columns with High Strength Steel and Concrete](#). *Structures*, 8:213–226.
- [2] Thai, S., Thai, H.-T., Uy, B., Ngo, T. (2019). [Concrete-filled steel tubular columns: Test database, design and calibration](#). *Journal of Constructional Steel Research*, 157:161–181.
- [3] American Institute of Steel Construction (2016). *Specification for structural steel buildings AISC 360-16*. Chicago, IL, USA: AISC.
- [4] Standards Australia/Standards New Zealand (2017). *Composite structures-Composite steel-concrete construction in buildings AS/NZS 2327:2017*.
- [5] CEN (European Committee for Standardizations (2004). *Design of composite steel and concrete structures Part 1-1: General rules and rules for buildings*. Brussels, Belgium.
- [6] Uy, B. (2001). [Strength of short concrete filled high strength steel box columns](#). *Journal of Constructional Steel Research*, 57(2):113–134.
- [7] Uy, B. (2001). [Axial compressive strength of short steel and composite columns fabricated with high strength steel plate](#). *Steel and Composite Structures*, 1(2):171–185.
- [8] Sakino, K., Nakahara, H., Morino, S., Nishiyama, I. (2004). [Behavior of Centrally Loaded Concrete-Filled Steel-Tube Short Columns](#). *Journal of Structural Engineering*, 130(2):180–188.
- [9] Liu, D. (2005). [Tests on high-strength rectangular concrete-filled steel hollow section stub columns](#). *Journal of Constructional Steel Research*, 61(7):902–911.
- [10] Liu, D., Gho, W.-M., Yuan, J. (2003). [Ultimate capacity of high-strength rectangular concrete-filled steel hollow section stub columns](#). *Journal of Constructional Steel Research*, 59(12):1499–1515.
- [11] Yu, Q., Tao, Z., Wu, Y.-X. (2008). [Experimental behaviour of high performance concrete-filled steel tubular columns](#). *Thin-Walled Structures*, 46(4):362–370.
- [12] Liew, J. Y. R., Xiong, D. X., Zhang, M. H. (2011). Experimental studies on concrete filled tubes with ultra-high strength materials. In *Proceedings of the 6th International Symposium on Steel Structures, Seoul, Korea*, 377–384.
- [13] Xiong, M.-X., Xiong, D.-X., Liew, J. Y. R. (2017). [Axial performance of short concrete filled steel tubes with high- and ultra-high- strength materials](#). *Engineering Structures*, 136:494–510.
- [14] Xiong, M.-X., Xiong, D.-X., Liew, J. Y. R. (2017). [Flexural performance of concrete filled tubes with high tensile steel and ultra-high strength concrete](#). *Journal of Constructional Steel Research*, 132:191–202.
- [15] Khan, M., Uy, B., Tao, Z., Mashiri, F. (2017). [Behaviour and design of short high-strength steel welded box and concrete-filled tube \(CFT\) sections](#). *Engineering Structures*, 147:458–472.
- [16] Khan, M., Uy, B., Tao, Z., Mashiri, F. (2017). [Concentrically loaded slender square hollow and composite columns incorporating high strength properties](#). *Engineering Structures*, 131:69–89.
- [17] Chen, S., Zhang, R., Jia, L.-J., Wang, J.-Y., Gu, P. (2018). [Structural behavior of UHPC filled steel tube columns under axial loading](#). *Thin-Walled Structures*, 130:550–563.
- [18] Huang, Z., Li, D., Uy, B., Thai, H.-T., Hou, C. (2019). [Local and post-local buckling of fabricated high-strength steel and composite columns](#). *Journal of Constructional Steel Research*, 154:235–249.
- [19] Nguyen, T.-T., Thai, H.-T., Ngo, T., Uy, B., Li, D. (2021). [Behaviour and design of high strength CFST columns with slender sections](#). *Journal of Constructional Steel Research*, 182:106645.
- [20] Cai, Y., Su, M., Chen, X., Young, B. (2021). [High strength steel square and rectangular tubular stub columns infilled with concrete](#). *Journal of Constructional Steel Research*, 179:106536.
- [21] Thai, H.-T., Uy, B., Khan, M., Tao, Z., Mashiri, F. (2014). [Numerical modelling of concrete-filled steel box columns incorporating high strength materials](#). *Journal of Constructional Steel Research*, 102:256–265.

- [22] Tao, Z., Uy, B., Liao, F.-Y., Han, L.-H. (2011). [Nonlinear analysis of concrete-filled square stainless steel stub columns under axial compression](#). *Journal of Constructional Steel Research*, 67(11):1719–1732.
- [23] Phan, H. D. (2021). [Numerical analysis of seismic behavior of square concrete filled steel tubular columns](#). *Journal of Science and Technology in Civil Engineering (STCE) - NUCE*, 15(2):127–140.
- [24] Han, L.-H., Yao, G.-H., Tao, Z. (2007). [Performance of concrete-filled thin-walled steel tubes under pure torsion](#). *Thin-Walled Structures*, 45(1):24–36.
- [25] Tao, Z., Wang, Z.-B., Yu, Q. (2013). [Finite element modelling of concrete-filled steel stub columns under axial compression](#). *Journal of Constructional Steel Research*, 89:121–131.
- [26] Gardner, L., Yun, X. (2018). [Description of stress-strain curves for cold-formed steels](#). *Construction and Building Materials*, 189:527–538.
- [27] Rossi, B., Afshan, S., Gardner, L. (2013). [Strength enhancements in cold-formed structural sections — Part II: Predictive models](#). *Journal of Constructional Steel Research*, 83:189–196.
- [28] Yun, X., Gardner, L. (2018). [Numerical modelling and design of hot-rolled and cold-formed steel continuous beams with tubular cross-sections](#). *Thin-Walled Structures*, 132:574–584.
- [29] Huang, Z., Uy, B., Li, D., Wang, J. (2020). [Behaviour and design of ultra-high-strength CFST members subjected to compression and bending](#). *Journal of Constructional Steel Research*, 175:106351.
- [30] Lee, J., Fenves, G. L. (1998). [Plastic-Damage Model for Cyclic Loading of Concrete Structures](#). *Journal of Engineering Mechanics*, 124(8):892–900.
- [31] Lubliner, J., Oliver, J., Oller, S., Oñate, E. (1989). [A plastic-damage model for concrete](#). *International Journal of Solids and Structures*, 25(3):299–326.
- [32] Grassl, P., Jirásek, M. (2006). [Damage-plastic model for concrete failure](#). *International Journal of Solids and Structures*, 43(22-23):7166–7196.
- [33] American Concrete Institute (2019). *Building Code Requirements for Structural Concrete and Commentary (ACI 318-19)*.
- [34] Hognestad, E. (1951). *Study of combined bending and axial load in reinforced concrete members*.
- [35] Samani, A. K., Attard, M. M. (2012). [A stress–strain model for uniaxial and confined concrete under compression](#). *Engineering Structures*, 41:335–349.
- [36] Tasdemir, M. A., Tasdemir, C., Akyüz, S., Jefferson, A. D., Lydon, F. D., Barr, B. I. G. (1998). [Evaluation of strains at peak stresses in concrete: A three-phase composite model approach](#). *Cement and Concrete Composites*, 20(4):301–318.
- [37] Binici, B. (2005). [An analytical model for stress–strain behavior of confined concrete](#). *Engineering Structures*, 27(7):1040–1051.
- [38] American Concrete Institute (1992). *Cracking of Concrete Members in Direct Tension ACI 224.2R-92 (Reapproved 2004)*.
- [39] Hillerborg, A., Modéer, M., Petersson, P.-E. (1976). [Analysis of crack formation and crack growth in concrete by means of fracture mechanics and finite elements](#). *Cement and Concrete Research*, 6(6): 773–781.
- [40] fib-federation internationale du (2010). *fib Model Code for Concrete Structures 2010*. John Wiley & Sons.
- [41] Mansur, M. A., Islam, M. M. (2002). [Interpretation of Concrete Strength for Nonstandard Specimens](#). *Journal of Materials in Civil Engineering*, 14(2):151–155.
- [42] Aslani, F., Uy, B., Tao, Z., Mashiri, F. (2015). [Behaviour and design of composite columns incorporating compact high-strength steel plates](#). *Journal of Constructional Steel Research*, 107:94–110.
- [43] Yan, Y., Xu, L., Li, B., Chi, Y., Yu, M., Zhou, K., Song, Y. (2019). [Axial behavior of ultra-high performance concrete \(UHPC\) filled stocky steel tubes with square sections](#). *Journal of Constructional Steel Research*, 158:417–428.
- [44] Varma, A. (2000). *Seismic behavior, analysis, and design of high strength square concrete filled steel tube (CFT) columns*. Lehigh University.
- [45] Ibañez, C., Hernández-Figueirido, D., Piquer, A. (2018). [Shape effect on axially loaded high strength CFST stub columns](#). *Journal of Constructional Steel Research*, 147:247–256.